Measurement of friction-induced changes in pig aorta fibre organization by non-invasive imaging as a model for detecting the tissue response to endovascular catheters

Luciana E Bostan[1#], Christopher Noble[2], Nicole Smulders[4], Roger Lewis[3], Matt J Carré[3], Steve Franklin[3,4], Nicola H Green[1*], Sheila MacNeil[1]

[1]*Department of Materials Science and Engineering, The Kroto Research Institute, North Campus, University of Sheffield, Broad Lane, Sheffield, S3 7HQ, United Kingdom*

[2]*CISTIB, Centre for Computational Imaging and Simulation Technologies in Biomedicine, INSIGNEO Institute for in silico Medicine, Department of Frictional Engineering, The University of Sheffield, Sheffield, UK*

[3]*Department of Frictional Engineering, The University of Sheffield, Mappin Street, Sheffield S1 3JD, United Kingdom*

[4]*Philips Research, Eindhoven, Netherland*

**Corresponding author*

Corresponding author contact details

email: n.h.green@sheffield.ac.uk

tel: 0114 2223932

fax: 0114 2225943

Keywords

catheterization; friction; confocal microscopy; non-invasive imaging; second harmonic generation

[#] Current address: Department of Molecular and Cell Biology, University of Leicester, University Road, Leicester, LE1 7RH, UK

Abstract

Alterations in quantity or architecture of elastin and collagen fibres are associated with some blood vessel pathologies. Also some medical interventions such as endovascular catheterization have the potential to damage blood vessels. This study reports the use of porcine aorta as a model system for studying the physical impact of catheters on vasculature, in conjunction with non-invasive imaging techniques to analyse collagen and elastin fibre organization and assess load-induced changes. Porcine aorta was exposed to frictional trauma and elastin and collagen fibre orientation evaluated by destructive, histochemical methods and non-invasive imaging. The latter allowed the immediate impact of force on fibre orientation and fibre recovery to be evaluated longitudinally.

In normal aorta, elastin fibres are aligned at the surface, but become less aligned with increasing depth, showing no alignment by ~30 μm. Collagen fibres meanwhile appear aligned down to a depth of 35 μm. Changes in collagen and elastin fibre orientation in healthy pig aorta were detected by conventional destructive histology within 5 minutes of application of a sliding 10N load, while lesser loads had less impact. Good recovery of fibre orientation was observed within 20 minutes. Non-invasive imaging of *ex vivo* aorta tissue provides a good indication of the extent of fibre re-organization following frictional stress, at loads similar to those encountered during medical interventions such as catheterization. These results indicate that tissue deformation can occur from these procedures, even in healthy tissue, and highlight the potential for the development of an *in vivo* probe capable of monitoring vascular changes in patients.

1. Introduction

Vascular surgeons increasingly use sophisticated endovascular catheters to investigate and treat vascular complications (e.g., ablation catheters [1], and force controlled and haptic catheters [2-4]). In the hands of experienced surgeons, perforations of blood vessels with endovascular catheters are very rare, however many of the patients being treated potentially have diseased vessels; in these cases even experienced surgeons may find that the use of the endovascular catheters leads to some damage of blood vessels. The currently available catheter systems are sometimes difficult and slow to manipulate into position, thereby, reducing their ability to safely interact with the blood vessels insertion and decrease the likelihood of blood vessel damage. However, a reduction in friction also decreases the degree of haptic feedback, which provides the surgeon with valuable information about the progress of the procedure. In addition, the insertion of a catheter can increase the risk of platelet aggregation in blood flow [5], but, in most cases, the patient is provided with an appropriate dosage of heparin. Damage to the extracellular matrix (ECM) will require a wound healing response and if it goes wrong this can lead to fibrosis [6]. Thus manoeuvrability represents a critical design feature for these catheters [7]. This feature is highly dependent on minimising the coefficient of friction between the catheter and the blood vessels. In response to a frictional insult, fibre production and orientation can change. This is why it is important to look at both when assessing damage inflicted by rubbing a catheter along aortic tissue. A problem in improving endovascular catheter design is obtaining information on the extent of the damage to blood vessels which may occur when catheters are used. The vascular endothelial surface layer (ESL) is notoriously fragile and may undergo damage during catheterization and repair post catheterization. ESL assessment has not proved a useful biological indicator of catheter–induced damage. This is because in almost all cases, patients undergoing catheterization as a result of cardiovascular

disease may already have pre-existing damage to their glycocalyx. In addition, the endothelium of such patients is potentially more vulnerable to damage by the catheter [8].

Accordingly the approach taken in this study was to look beneath the ESL and examine the relationship between mechanical stress caused by friction (using materials used in endovascular catheter tips) and the deformation of collagen and elastin fibres in pig aorta tissue *ex vivo*.

Our aims in this study were to use an experimental system to apply loads similar to those occurring during endovascular catheterization; to examine whether there was a predictable change in collagen and elastin fibre organization related to the level of frictional stress applied; to examine the extent to which fibre deformation was permanent or recoverable and; most importantly, to explore the possibility of using non-invasive imaging technology to evaluate collagen content and fibre reorientation after frictional insult. The strength of the aorta depends on the organization of fibres in the ECM. In the aorta the adventitial layer contains mainly collagen, while the medial layer consists of collagen and elastin [9]. The orientation of collagen fibres is important in providing tensile strength while the elastin provides elasticity to tissues, allowing them to return to their original state post deformation [10].

In this study we first examined the effect of physical insult on collagen and elastin fibres in pig aorta by fixing the tissue post insult and characterizing the fibre orientation by haematoxylin and eosin staining. We then developed a holder which kept the aorta at a pre-stretched load and allowed the application of a single pass at a predetermined load, of a 4mm diameter sphere of PEBA (polyether block amide), commonly used in the manufacture of endovascular catheter tips. We used second harmonic generation (SHG) imaging and two photon excitation fluorescence (TPEF) to detect changes in the organization of the collagen and elastin fibres, respectively.

2. Materials and Methods

All chemicals were obtained from Sigma-Aldrich (Dorset, UK) unless otherwise stated.

2.1 Pig aorta preparation

Porcine hearts with aortas attached were purchased from a local butcher 24 h after slaughter and stored in phosphate buffered saline (PBS, Oxoid, Hampshire, UK) at 4°C for transportation, which generally took less than 1 h. On arrival at the laboratory, the aortas were immediately detached from the hearts with a scalpel and washed three times in sterile PBS. Pieces of aorta ~4 cm long were cut along the main axis to obtain rectangular, flat strips of aortic tissue, which could be stretched longitudinally.

On examination we found the retention of endothelial cells was very patchy and uneven – almost certainly due to trauma during handling (confirmed by silver nitrate staining for the endothelium - results not shown). Since we were unable to obtain fresh samples with intact endothelia and ESL assessment has not proved useful in the determination of catheter–induced damage [8], we focused on studying the impact of force on the collagen and elastin fibres of the aorta.

2.2 Friction test

Friction tests were carried out using a CETR-UMT 2 (Bruker, Massachusetts, USA) tribometer with the load stabilized for 20 s before testing. The friction test samples were immersed in a blood substitute solution (0.9 mM dextran 70, 155 mM NaCl) to replicate blood viscosity and rheological behaviour [11]. To mimic the *in vivo* state of the unpressurised aorta, a tissue sample holder was developed by Philips Research, Eindhoven, Netherlands and the West Pomeranian University of Technology, Szczecin, Poland to hold the aorta sample during the friction test and maintain uniaxial tension. This device has been described elsewhere [12]. The fresh pig aorta was flattened in the longitudinal direction, the sample length increased by 15

%, reflecting the degree of stretching observed during normal blood flow, and the sample held in place.

In the preliminary tests a catheter tip, made of a polymer matrix including PEBA (Boston Scientific 6F Guide Catheter (Massachusetts, USA) with 2.1 mm external diameter, 1.7 mm internal diameter) with a 'hollow tube' tip geometry, was held at 45° with respect to the friction surface during sliding. Normal loads in the range of 100 mN - 3 N were applied as a single pass along the longitudinal axis of the aorta, the samples were fixed within 10 minutes of the frictional insult, sectioned and haematoxylin and eosin (H&E) stained. Tests were also carried out with a 4mm diameter steel ball at 5 N.

Subsequent tests used an injection-moulded 4 mm diameter PEBA ball (Pebax® 3533, hardness ShD 33, courtesy of Philips Research, Eindhoven, Netherlands), held perpendicular to the plane of the tissue and driven once across the sample along the longitudinal axis, at 1 mm/s, with 1, 5 or 10 N applied normal load. Initially, the fibre response was analysed as before by fixing the tissue immediately after frictional insult. In addition some samples were allowed to rest for 90 minutes prior to fixing to evaluate fibre recovery. In all cases these samples were H&E stained.

In the final experiments, the fixing and staining procedure was replaced by non-invasive imaging of the samples with a confocal microscope since this facilitated repeated imaging of the same area during the recovery process.

2.3 Preparation of histological sections

The samples were fixed in 10% formaldehyde solution, processed and embedded in paraffin blocks. Three 5µm thick sections were cut from each block and stained with haematoxylin and eosin.

2.4 Confocal imaging

Collagen was visualized within the samples by SHG imaging in the epi-direction at different depths using a Zeiss LSM 510 Meta upright laser-scanning confocal microscope (Oberkochen, Germany) attached to a tunable (700–1060 nm) Chameleon Ti:sapphire multiphoton laser (Coherent, CA, USA). For TPEF imaging of elastin, the illumination wavelength was 800 nm and intrinsic fluorescence was detected between 447 and 597nm. Collagen SHG signals were obtained using 950 nm illumination and collected using a 10 nm band pass filter centred on 475 nm [13,14]. All imaging was performed using a 40x 1.3 NA oil immersion objective. The elastin TPEF was collected using λex 800nm and λem 447 - 597 nm, avoiding any potential collagen SHG signal at 400 nm, while collagen SHG was detected by λex 950nm, λem 470-480 nm. Images of the two components were collected sequentially from the same area. It is important to note that although collagen and elastin overlap in their TPEF excitation and emission spectra, they can be readily distinguished since only collagen produces SHG.

To ensure that the same area was imaged before and after load application, the sample holder described above was placed at the same position using the microscope XY stage. For each sample, about 35 µm thickness of the vessel wall was imaged and a z stack of images at 1 µm intervals was generated.

Non-invasive imaging was also employed in conjunction with enzymatic treatments to confirm the nature of the signals detected and ascertain the effective of fibre removal on the orientation of the remaining fibres within the tissue.

2.5 Enzymatic treatment of collagen and elastin

Tissues were treated enzymatically to disrupt the collagen or elastin architecture to verify the source of the SHG and TPEF signals. Samples were immersed in PBS solution with antibiotics (Penicillin and Streptomycin) and fungicide, to prevent growth of micro- organisms and were

treated with either collagenase A (0.120 U/ml) or elastase (0.011 U/ml). Samples were then incubated for 20 hours at 37°C to ensure digestion of the relevant proteins.

2.6 Characterizing the collagen and elastin fibres orientation

Mean fibre direction was extracted from SHG and TPEF images based on 2D Fourier transform analysis using ImageJ [15] and the Directionality plug-in created by Jean-Yves Tinevez (http://pacific.mpi-cbg.de/wiki/index.php/Directionality) following the online instructions. Images were converted into greyscale and the angle of each fibre was analysed by Fast Fourier Transform, producing a directionality histogram in which all fibres were mapped for directionality against a scale of 0 to 180°. The orientation of the fibres was analysed from z-stack images, producing a histogram with the peak indicative of the dominant orientation.

3. Results

3.1 Friction test

The friction behaviour of a PEBA ball was investigated. Lubricants or gel-like materials with a hydrophilic polymer surface have been developed and used in order to provide lubricity to the endovascular catheter tips. Usually, they are designed to give a low COF when in contact with the vessel wall in order to minimize trauma and tissue irritation [12; 16]. Estimations of the contact pressure and the area of contact were made using the Hertzian contact model. This involved assigning parametric values of 0.4 and 0.5 for the Poisson ratio of the probe and for pig aorta, respectively, 14.6 MPa and 0.043 MPa for the elastic modulus [17]. The estimated contact pressure was 0.05, 0.09 and 0.1 MPa for 1, 5 and respectively 10N and the contact area diameter was 5.93, 10.13 and 12.76 mm respectively for 1, 5 and 10N.

The COF results indicated that this decreased with increasing force (Figure 1). COF is a measure of the surface interactions between the two contacting bodies. As materials slide

against each other, the materials interact with each other. The actual frictional force can result from a variety of mechanisms such as: adhesion, deformation, and hysteresis. As the load increases contact area and ploughing increase and the resulting energy dissipation due to adhesion and deformation mechanism increases in concert with frictional force to increase [18]. A threshold load typically exists above which the material cannot be compressed further, leading to a non-linear rise in friction force with applied normal force and therefore COF decreases.

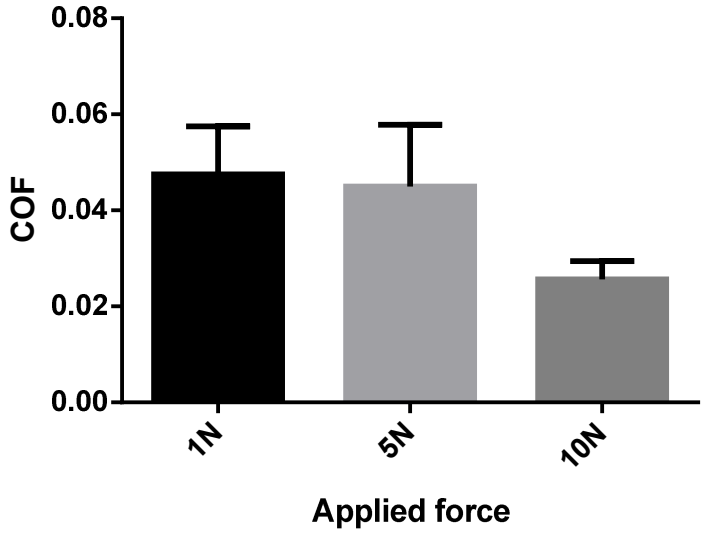

Figure 1: Average friction behaviour of PEBA ball
The average friction behaviour of the PEBA ball when applied to pig aorta at normal loads between 1 and 10 N. The ball was moved across the sample at 1 mm/s; the error bars indicate the SEM derived from at least four individual experiments.

3.2 Histological observation of pig aorta ECM fibres following frictional insult

Preliminary tests using a catheter tip and loads between 100 mN and 3N demonstrated that it was possible to detect a reorganization of the H&E stained fibres after a single pass with this tip and this was most noticeable when a load of 400mN was applied (Figure 2).

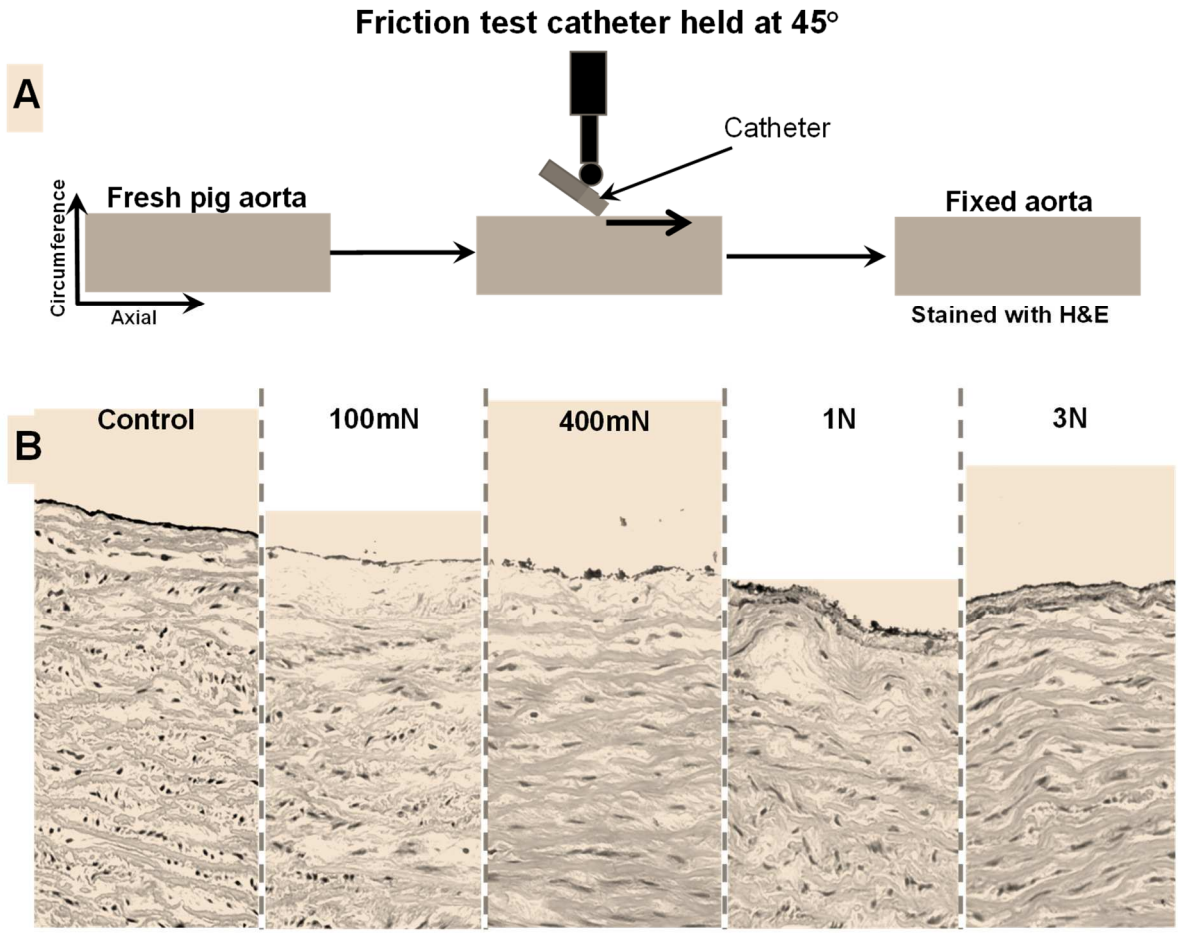

Figure 2: The effect of friction from a catheter tip on fibres in the aorta
Pig aortas were freshly excised and subjected to minimal stretching to flatten them out. Loads of 100 mN, 400 mN, 1 N and 3 N were applied from a single pass of a catheter held at 45° at a constant speed of 1 mm/s (A). Tissue was then fixed, sectioned and stained with H&E (B). Images shown are at 20x magnification.

This preliminary data also suggested that reorganization of fibre orientation could be detected in response to a single friction pass of a steel ball (at 5 N) (Figure 3).

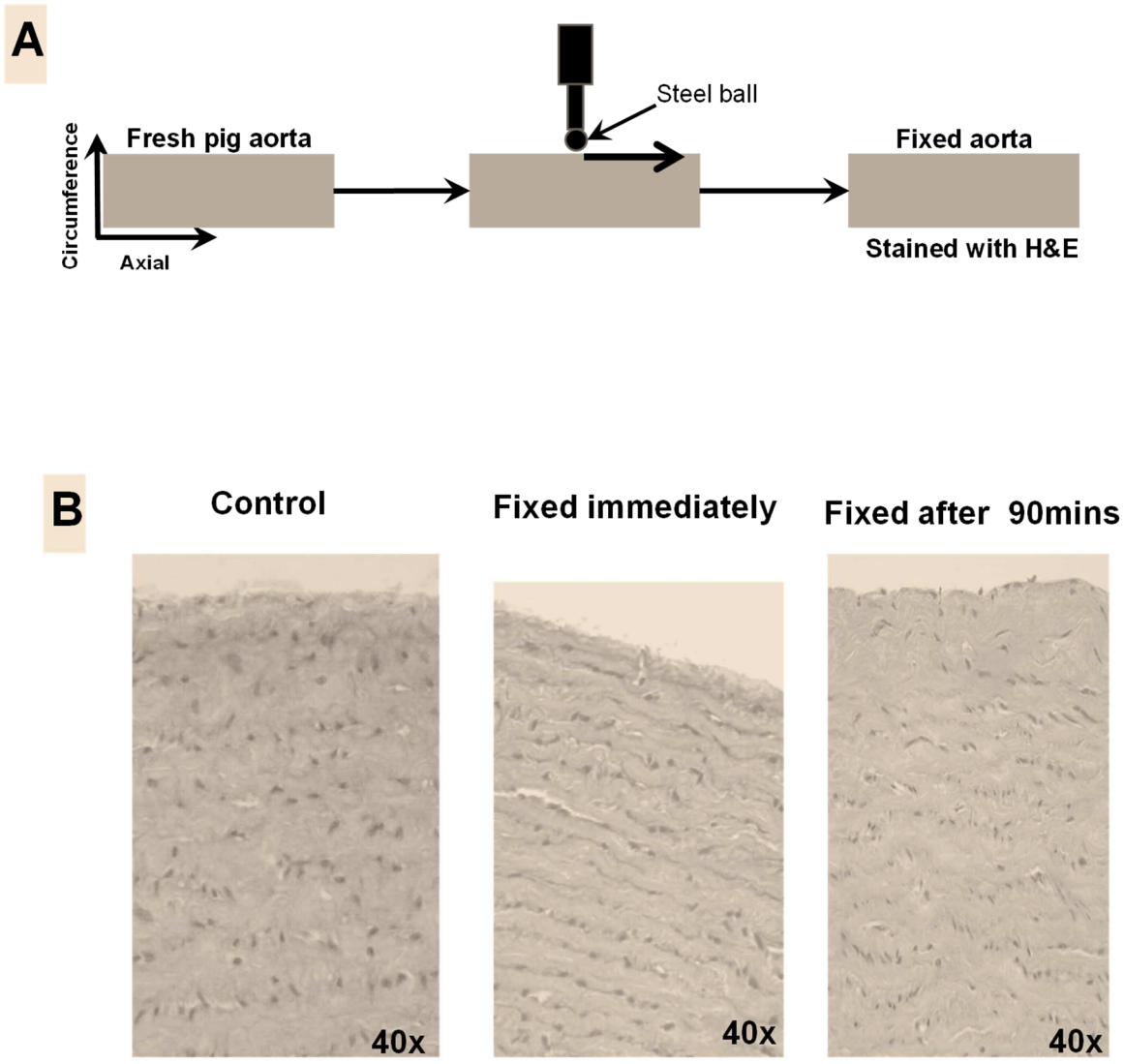

Figure 3: The effect of friction from a steel ball on fibres in the aorta
Pig aortas were freshly excised and subjected to minimal stretching of 15% to flatten them out. 5 N load was applied using a 4 mm diameter steel ball at a constant speed of 1mm/s (A). In these experiments, tissues were subjected to 5 N in a single pass of a steel ball and then either fixed within 10 minutes or allowed to stand for 90 minutes before fixing. With H&E staining (Figure 3B) a flattening of all fibres immediately after the frictional insult and recovery after 90 minutes prior to fixation was observed.

3.3 Non-invasive imaging of collagen and elastin fibres

To reduce the impact of sample processing and to investigate the changes throughout the sample in more detail, the collagen and elastin fibre arrangement was examined by non-invasive imaging methods.

SHG and TPEF images of the collagen and elastin fibres respectively were obtained non-invasively at 1 µm depth intervals for a 30 µm z stack (Figure 4).

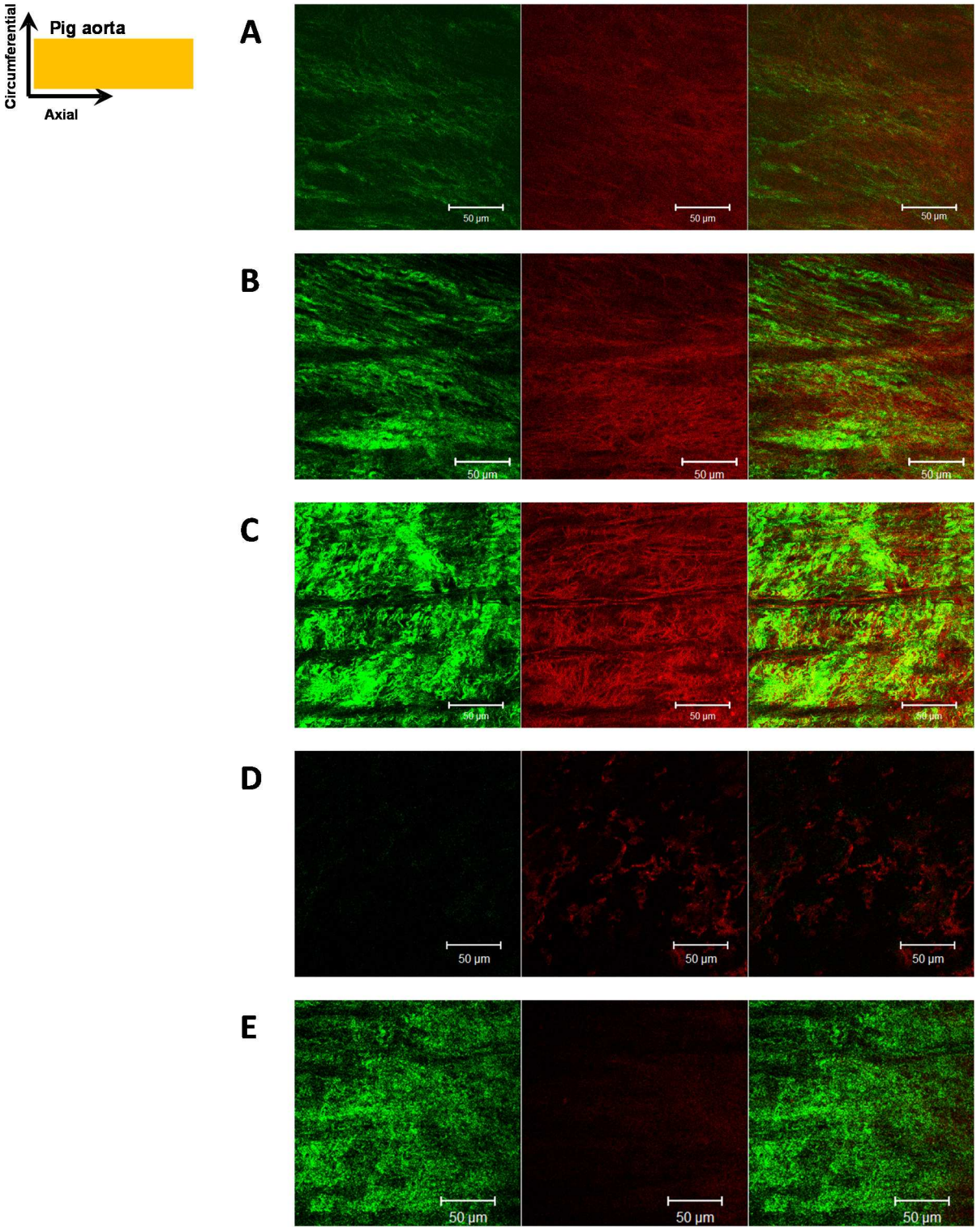

Figure 4: Orientation of collagen and elastin fibres in relaxed pig aorta before friction test. Images show collagen (SHG - green) and elastin (TPEF - red) fibres separately and as a combined image. The relaxed sample (A) shows relatively little alignment of collagen

and elastin at the surface. At depths up to 25 µm (B) there is considerable co-alignment of collagen and elastin, while beyond 25 µm (C) alignment of collagen and elastin differs. The tissue was then treated with collagenase (D) or elastase (E) and imaged as before to confirm the identity of the components detected.

3.4 Collagenase and elastase treatment of porcine aorta prior to friction insult

To confirm the nature of the components detected by SHG and TPEF, the impact of enzymatic digestion of the two components on non-invasive imaging was determined. Samples were treated with collagenase A or elastase and compared to the untreated control. All images were obtained using the same imaging parameters, as previously described. The fibre orientation was then determined (Figure 6).

The collagen fibre angle appears mostly unchanged (Figure 5B) compared to the control (Figure 5A); this could be speculated to indicate the homogeneous break down of the collagen fibres. The arrangement of the collagen fibres also appears to change following elastase treatment: the previously tight bundles appear rippled, more diffuse and with a clear single directionality (Figure 5C), not present in control samples, indicating the interconnectivity between the elastin and collagen networks.

Elastin structure in the collagenase treated samples was greatly altered compared to the control, possibly resulting from detachment of the elastin from the collagen network. Following elastase treatment, the images show a clear loss of elastin, compared to the controls, and there appears to be little remaining structure. Furthermore, the elastin fibre angle is greatly altered, with less clear directionality (Figure 5F). However this may be due to the loss of remaining structure such that no clear fibre angle could be detected. Noble *et al*. previously reported that collagenase and elastase treatment of porcine aorta alters the uniaxial tension response [19]. Therefore this may provide insight into the change observed in that study.

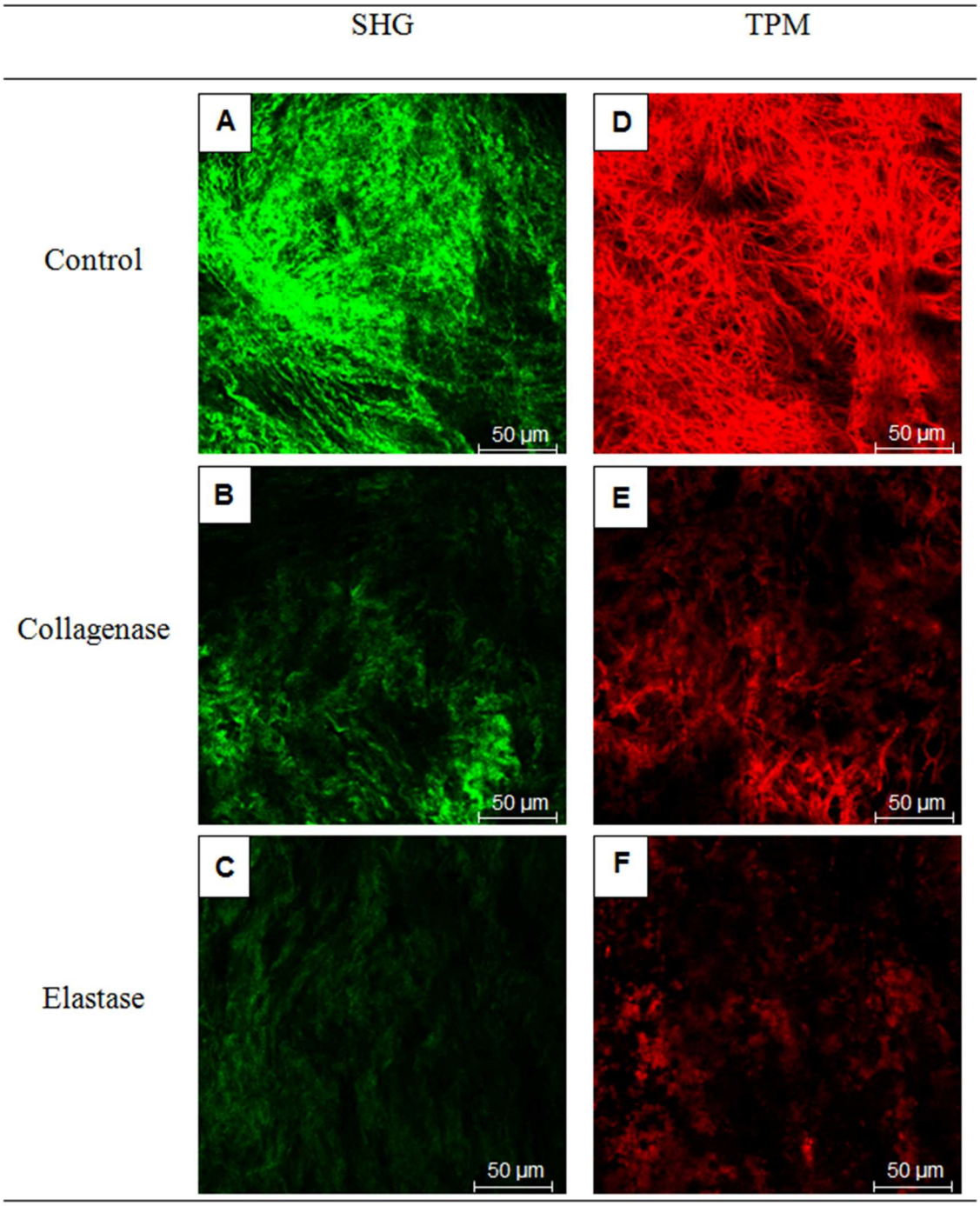

Figure 5: Images of collagen and elastin fibres after enzymatic digestion.

Images were obtained by increasing amplifier gain, from a depth of 16.5 µm from the surface of the intima, for control (A, D), collagenase (B, E) and elastase (C, F) treated samples. Scale bar = 50 µm.

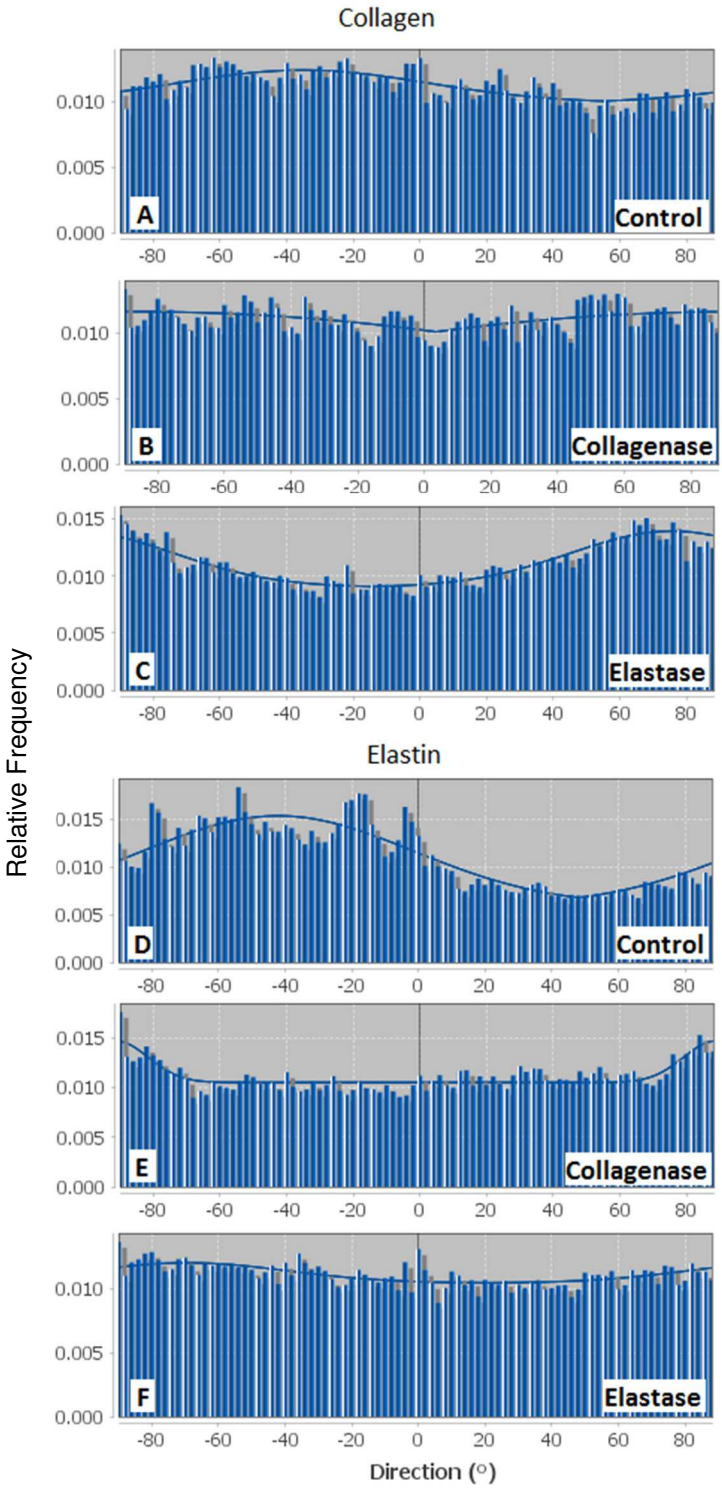

Figure 6: Collagen and elastin fibre directionality histograms for samples in figure 5 (D and E). Collagen (A-C) and elastin (D-F) fibre angle versus relative frequency illustrates the predominant fibre direction. 0 is the axial direction and ±90˚ is the circumferential direction. Samples are control (A, D), collagenase (B, E) and elastase (C, F) treated.

The collagen fibre angle (with collagenase) appears mostly unchanged (Figure 6B) compared to the control (Figure 6A); this could be speculated to indicate the homogeneous break down of the collagen fibres. The arrangement of the collagen fibres also appears to change following elastase treatment: the previously tight bundles appear rippled, more diffuse and with a clear single directionality (Figure 6C), not present in control samples, indicating the interconnectivity between the elastin and collagen networks.

Elastin structure in the collagenase treated samples was greatly altered compared to the control, possibly resulting from detachment of the elastin from the collagen network. The predominant -40˚ orientation, seen in the control samples (Figure 6D), is lost and ±90˚ orientation dominates (Figure 5E). Following elastase treatment, the images show a clear loss of elastin, compared to the controls, and there appears to be little remaining structure. Furthermore, the elastin fibre angle is greatly altered, with less clear directionality (Figure 6F). However this may be due to the loss of remaining structure such that no clear fibre angle could be detected. Noble *et al*. previously reported that collagenase and elastase treatment of porcine aorta alters the uniaxial tension response [19]. Therefore this may provide insight into the change observed in that study.

3.5 Imaging of collagen and elastin fibre orientation following frictional insult

Fibre orientation versus depth of aorta was determined for both elastin and collagen. The directionality was recorded before samples were stretched and then 5, 10, 20 and 30 minutes after stretching. No difference was observed in relation to stretching time prior to imaging (data not shown).

The relationship between load and fibre orientation was examined in pig aortas subjected to loads of 1, 5 and 10 N (Figure 7).

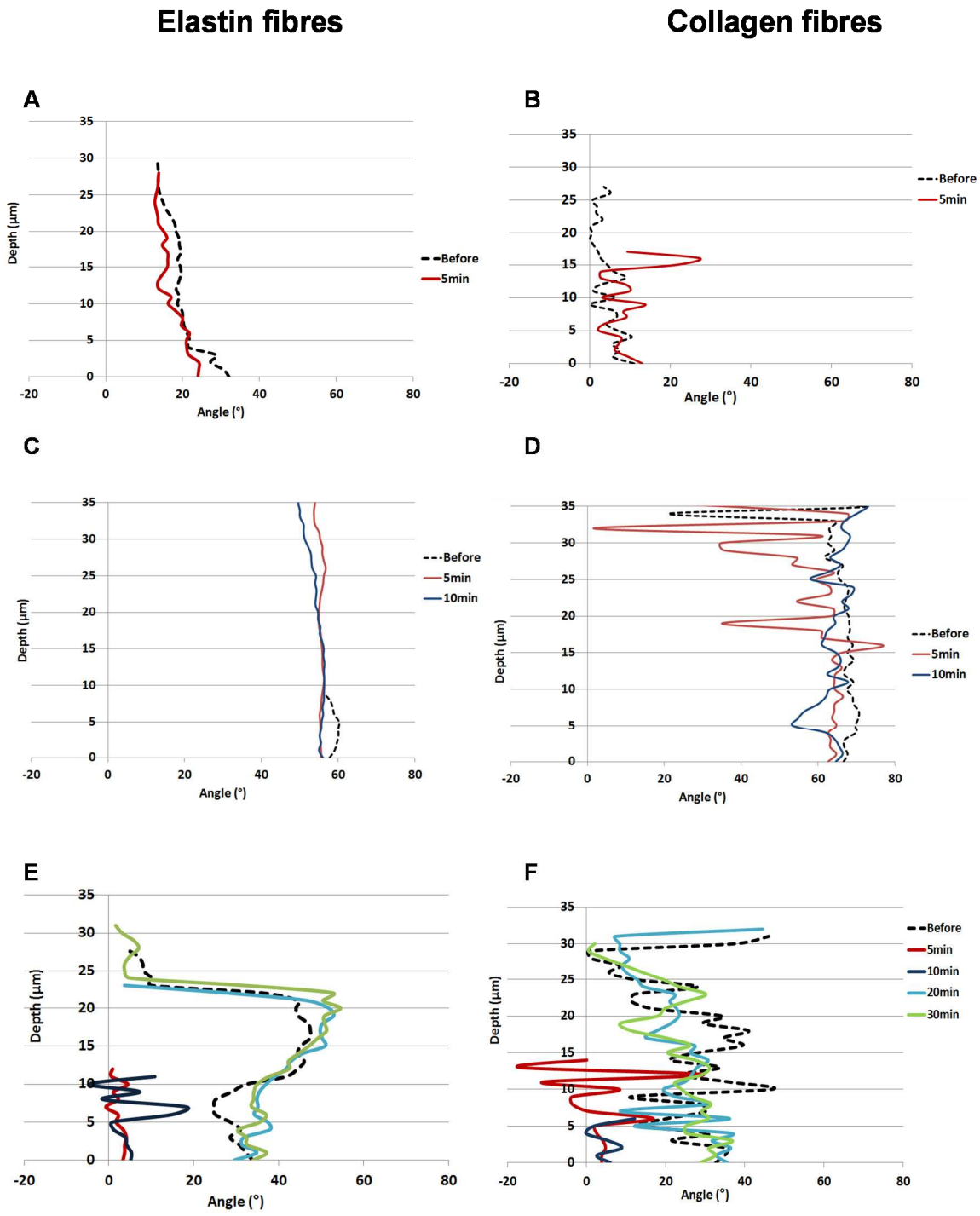

Figure 7: Fibre orientation in aorta before and after longitudinal loading
Pig aortas were held in the restraining device and subject to 15% stretching prior to the application of 1 N (A and B), 5 N (C and D) or 10 N (E and F) loads in a single pass. The dotted line shows the orientation of the fibres before load and the red, dark blue, light blue and green lines show the orientation of the fibres 5, 10, 20 and 30 minutes post loading, respectively. A, C and E show the results for elastin fibres and B, D and F show the collagen fibres.

With 1N there was no detectable change in the orientation of the fibres 5 minutes after applying the single pass load (Figure 7A, B). For a 5 N load there was no detectable change in the elastin and a very slight change in the collagen orientation that recovered within 10 minutes (Figure 7B, C). However, with 10 N there was a dramatic change in the orientation of both the elastin and the collagen fibres within 5 minutes of applying the load (Figure 7E, F). After 10 minutes there was no recovery in fibre alignment for either elastin or collagen but by 30 minutes the fibre orientation had recovered completely.

4. Discussion

The aim of this study was to investigate the possibility of using non-invasive SHG and TPEF imaging to detect the effect of a sliding load on pig aorta to simulate the forces generated by the insertion of endovascular catheters. To achieve this we used an experimental system, developed previously by the authors [19] to determine methodologies for applying loads reproducibly and analysing the response of the tissue to normal and frictional loading through non-invasive imaging.

The techniques of SHG and TPEF have been previously used to investigate collagen and elastin networks, respectively, in arteries [10, 20] heart valves [12, 21] porcine cartilage [22] and skin [23].

Animal blood vessels in the form of a pig aorta, were chosen for this study since obtaining diseased human tissue in sufficient quantities is very difficult (both practically and ethically). Moreover, it has been found that pig blood vessels have similar behaviour to human blood vessels [24].

Results indicated that fresh pig aorta responded predictably to increasing loads (single pass) with a temporary change in the orientation of the collagen and elastin fibres. At low loads of 1 and 5N there was very little change, while at the higher load load of 10 N there was

considerable realignment. Both collagen and elastin fibres within 5 minutes of loading. It is interesting to note that these changes in collagen and elastin fibre orientation were partially restored within 20 minutes, with a complete return to the original alignment within 30 minutes. We hypothesize that both changes in alignment of fibres and the rate of recovery relate to the extent of the load applied, although additional studies are needed to investigate this further.

A major contribution of this study is demonstrating that dynamic and reversible changes in collagen and elastin fibre orientation can be detected non-invasively, by SHG and TPEF respectively. The images obtained facilitated analysis of the orientation of the fibres at different depths in the aortic tissue and allowed the detection of changes in their orientation and response to load and the measurement of recovery over a period of 30 minutes.

SHG imaging is a minimally invasive, non-linear, two-photon based technique requiring no sample preparation, generated when non-centrosymmetric structures are illuminated with focused laser light in an ultrashort pulse. Collagen is a strong SHG source [25, 26] and by using near infrared wavelengths for the incident light, SHG imaging has the ability to penetrate deeper into thick tissue, producing single plane images that can be re-constructed into three dimensional images [27]. Consequently it is an ideal technique for non-destructively monitoring tissues. However, despite these advantages, it is only over the last few years that SHG imaging of collagen structures in tissue has begun to be adopted more widely. A recent review was published on the development and burgeoning use of SHG imaging in the clinic to investigate collagen remodelling in cancer in *ex vivo* and *in vivo* human tissue [28]; changes in collagen structure during fibrosis are also being monitored; *ex vivo* in humans, *in vivo* in animals, by SHG imaging [29-31]. In addition SHG imaging is now playing an important role in non-invasive imaging of collagen structure, formation and remodelling in tissue engineering and regenerative medicine, as reviewed recently by Vielreciher *et al*. [32].

Changes to elastin and collagen fibres in the enzyme-treated samples may alter the frictional response of the tissue. Noble *et al*. performed uniaxial tensile testing of collagenase and elastase treated samples to create a model of diseased aorta [19]. They report weakening of collagenase treated samples in the axial direction. This behaviour may be explained by the results of this study since collagenase treatment resulted in the breakdown of collagen fibres, known to provide resistance at high strain, together with changes to elastin structure and orientation, which may have affected the attachment and subsequent recruitment of the remaining collagen fibres. Noble *et al*. also found elastase-treated samples had increased compliance in both directions. Our study suggests that this may be due to both loss of elastin and changes to collagen fibre structure. This work therefore supports the assertions of that study that these treatments provide a basis for the creation of models of disease aorta.

The effect of such treatments on the loading response of the tissue was not investigated here. However application of the loading applied in this study to enzyme treated artery would provide further assessment of the model proposed for emulating diseased tissue frictional properties.

Recent studies have demonstrated the development of an endoscopic probe capable of obtaining *in vivo* SHG images of murine cervical tissue [33], with the potential to be used in the clinical assessment of abnormal collagen remodeling within the cervix associated with preterm birth. As our study demonstrates, changes in collagen and elastin fibre orientation in response to frictional load can also be imaged non-destructively through the collection of SHG and endogenous fluorescence signals, and without the need for additional staining or contrast agents. Consequently a similar *in vivo* probe could be developed to measure the impact of physical trauma during medical interventions such as catheterization. This technology could also be useful in the assessment of pathological conditions of the aorta and other blood vessels

characterized by changes in the quantity and/or architecture of the elastin and collagen fibres such as aneurysms, atherosclerosis or genetic disorders [34, 35].

5. Conclusions

Endovascular catheterisation has the potential to damage blood vessels. Non-invasive imaging provides reliable indication of fibre re-organisation following mechanical insult. Recovery of the collagen and elastin fibre orientation was observed within 20 minutes. The techniques used are minimally invasive, requiring no sample preparation, and often the potential to develop an in vivo probe for monitoring vascular changes.

Acknowledgements

We gratefully acknowledge support for this research from the European Commission FP7 project UNITISS, FP7-PEOPLE-2011-IAPP/286174.

References

1**. Barnett, A.S., Bahnson, T.D., Piccini, J.P.:** Recent Advances in Lesion Formation for Catheter Ablation of Atrial Fibrillation, Circ Arrhythm Electrophysiol, **9**, 1-5 (2016).

2. **Providência, R., Marijon, E., Combes, S., Bouzeman, A., Jourda, F., Khoueiry, Z., Cardin, C., Combes, N., Boveda, S., Albenque, J.P.:** Higher contact-force values associated with better mid-term outcome of paroxysmal atrial fibrillation ablation using the SmartTouch™ catheter, Europace, **17**, 56–63 (2015).

3. **Natale, A., Reddy, V.Y., Monir, G., Wilber, D.J., Lindsay, B.D., McElderry, H.T., Kantipudi, C., Mansour, M.C., Melby, D.P., Packer, D.L., Nakagawa, H., Zhang, B., Stagg, R.B., Boo, L.M., Marchlinski, F.E.:** Paroxysmal AF Catheter Ablation With a Contact Force Sensing Catheter, Results of the Prospective, Multicenter SMART-AF Trial. J Am Coll Cardiol., **64**, 647–56 (2014).

4. **Kesner, S.B. and Howe, R.D.:** Discriminating Tissue Stiffness with a Haptic Catheter: Feeling the Inside of the Beating Heart, Joint Eurohaptics Conf Symp Haptic Interfaces Virtual Environ Teleoper Syst, 13-18 (2011).

5. **Tian**, X., **Sun**, A., **Liu**, X., **Pu**, F., **Deng**, X., **Kang**, H., **Fan**, Y.: Influence of catheter insertion on the hemodynamic environment in coronary arteries, Med Eng Phys, 38(9), 946-951 (2016).

6. **Mutsaers, S.E., Bishop, J.E., McGrouther, G., and Laurent, G.J.:** Mechanisms of tissue repair: from wound healing to fibrosis, Int. J. Biochem. Cell Biol., **29**, 5-17 (1997).

7. **Dellimore, K., Franklin, S., and Helyer, A.:** A Review of Catheter Related Complications During Minimally Invasive Transcatheter Cardiovascular Intervention with Implications for Catheter Design, Cardiovasc Eng Tech, **5**, 217-232 (2014).

8. **Sobolewski, P. and El, F.M.:** Cardiac catheterization: consequences for the endothelium and potential for nanomedicine, Wiley. Interdiscip. Rev. Nanomed. Nanobiotechnol., **7**, 458-473 (2015).

9. **Holzapfel, G.A., Gasser, T.C., and Ogden, R.W.:** A new constitutive framework for arterial wall mechanics and a comparative study of material models, Journal of Elasticity, **61**, 1-48 (2000).

10. **Zoumi, A., Lu, X., Kassab, G.S., and Tromberg, B.J.:** Imaging coronary artery microstructure using second-harmonic and two-photon fluorescence microscopy, Biophys. J., **87**, 2778-2786 (2004).

11. **Liepsch, D., Thurston, G., and Lee, M.:** Studies of fluids simulating blood-like rheological properties and applications in models of arterial branches, Biorheology, **28**, 39-52 (1991).

12. **Niemczyk, A., El Fray, M., and Franklin, S.E.:** Friction behaviour of hydrophilic lubricious coatings for medical device applications, Tribology International, **89**, 54-61 (2015).

13. **Campagnola, P.J. and Loew, L.M.**: Second-harmonic imaging microscopy for visualizing biomolecular arrays in cells, tissues and organisms, Nat. Biotechnol., 21, 1356-1360 (2003).

14. **Konig, K., Schenke-Layland, K., Riemann, I., and Stock, U.A.:** Multiphoton autofluorescence imaging of intratissue elastic fibres, Biomaterials, **26**, 495-500 (2005).

15. **Schneider, CA., Rasband, WS., and Eliceiri, KW.:** NIH Image to ImageJ: 25 years of image analysis, Nature Methods, **9**, 671-675 (2012).

16. **Nagaoka**, S., **Akashi**, R.: Low-friction hydrophilic surface for medical devices, Biomat, 11,;:419–24, (1990).

17. **Fung**, Y., C.: Biomechanics-Mechanical Properties of Living Tissues, Springer-Verlag New York, ISBN 978-1-4757-2257-4 (1993).

18. **Kwiatkowska, M., Franklin, S.E., Hendriks, C.P, Kwiatkowskia, K.:** Friction and deformation behaviour of human skin, Wear, 267, 1264-1273 (2009).

19. **Noble, C., Smulders, N., Green, N.H., Lewis, R., Carré, M.J., Franklin, S.E., MacNeil, S., and Taylor, Z.A.:** Creating a model of diseased artery damage and failure from healthy porcine aorta, Journal of the Frictional Behaviour of Biomedical Materials, **60**, 378-393 (2016).

20. **Boulesteix, T., Pena, A.M., Pages, N., Godeau, G., Sauviat, M.P., Beaurepaire, E., and Schanne-Klein, M.C.:** Micrometer scale ex vivo multiphoton imaging of unstained arterial wall structure, Cytometry A, **69**, 20-26 (2006).

21. **Schenke-Layland, K., Riemann, I., Opitz, F., Konig, K., Halbhuber, K.J., and Stock, U.A.:** Comparative study of cellular and extracellular matrix composition of native and tissue engineered heart valves, Matrix Biol., **23**, 113-125 (2004).

22. **Brockbank, K.G., MacLellan, W.R., Xie, J., Hamm-Alvarez, S.F., Chen, Z.Z., and Schenke-Layland, K.:** Quantitative second harmonic generation imaging of cartilage damage, Cell Tissue Bank., **9**, 299-307 (2008).

23. **Seidenari, S., Arginelli, F., Bassoli, S., Cautela, J., French, P.M., Guanti, M., Guardoli, D., Konig, K., Talbot, C., and Dunsby, C.:** Multiphoton laser microscopy and fluorescence lifetime imaging for the evaluation of the skin, Dermatol. Res. Pract., **2012**, 810749 (2012).

24. **Li**, W. C.: "Biomechanical properties of ascending aorta and pulmonary trunk in pigs and humans." Xenotransplantation 15(6): 384-389 (2008).

25. **Cox, G. and Kable, E.:** Second-harmonic imaging of collagen, Methods Mol. Biol., **319**, 15-35 (2006).

26. **Zipfel, W.R., Williams, R.M., Christie, R., Nikitin, A.Y., Hyman, B.T., and Webb, W.W.:** Live tissue intrinsic emission microscopy using multiphoton-excited native fluorescence and second harmonic generation, Proc. Natl. Acad. Sci. U. S. A, **100**, 7075-7080 (2003).

27. **Bianchini, P. and Diaspro, A.:** Three-dimensional (3D) backward and forward second harmonic generation (SHG) microscopy of biological tissues, J. Biophotonics., **1**, 443-450 (2008).

28. **Perry, S.W., Burke, R.M., and Brown, E.B.:** Two-Photon and Second Harmonic Microscopy in Clinical and Translational Cancer Research, Ann. Biomed. Eng, (2012).

29. **Pena, A.M., Fabre, A., Debarre, D., Marchal-Somme, J., Crestani, B., Martin, J.L., Beaurepaire, E., and Schanne-Klein, M.C.:** Three-dimensional investigation and scoring

of extracellular matrix remodeling during lung fibrosis using multiphoton microscopy, Microsc. Res. Tech., **70**, 162-170 (2007).

30. **Strupler, M., Hernest, M., Fligny, C., Martin, J.L., Tharaux, P.L., and Schanne-Klein, M.C.:** Second harmonic microscopy to quantify renal interstitial fibrosis and arterial remodeling, J. Biomed. Opt., **13**, 054041 (2008).
31. **Sun, W., Chang, S., Tai, D.C., Tan, N., Xiao, G., Tang, H., and Yu, H.:** Nonlinear optical microscopy: use of second harmonic generation and two-photon microscopy for automated quantitative liver fibrosis studies, J. Biomed. Opt., **13**, 064010 (2008).
32. **Vielreicher, M., Schurmann, S., Detsch, R., Schmidt, M.A., Buttgereit, A., Boccaccini, A., and Friedrich, O.:** Taking a deep look: modern microscopy technologies to optimize the design and functionality of biocompatible scaffolds for tissue engineering in regenerative medicine, J. R. Soc. Interface, **10**, 20130263 (2013).
33. **Zhang, Y., Akins, M.L., Murari, K., Xi, J., Li, M.J., Luby-Phelps, K., Mahendroo, M., and Li, X.:** A compact fibre-optic SHG scanning endomicroscope and its application to visualize cervical remodeling during pregnancy, Proc. Natl. Acad. Sci. U. S. A, **109**, 12878-12883 (2012).
34. **Antanas, M., John Chan, K.M., Patni, R., Nawaz, M.A., Punjabi, P.P., and Macys, A.:** Ascending aortic aneurysms: pathophysiology and indications for surgery, ESC Council for Cardiology Practice, **10**, Nº 7 (2011).
35. **Wiernicki, I., Cnotliwy, M., Baranowska-Bosiacka, I., Urasinska, E., Kwas, A., Bober, J., and Gutowski, P.:** Elastin degradation within the abdominal aortic aneurysm wall--relationship between intramural pH and adjacent thrombus formation, Eur. J. Clin. Invest, **38**, 883-887 (2008).